VOL. 6, NO. 7, JULY 2011 ISSN 1819-6608
ARPN Journal of Engineering and Applied Sciences

www.arpnjournals.com

NUMERICAL ANALYSIS OF FIN-TUBE PLATE HEAT EXCHANGER BY USING CFD TECHNIQUE

Ahmed F. Khudheyer and Mahmoud Sh. Mahmoud
Department of Mechanical Engineering, Nahrain University, Baghdad, Iraq
E-Mail: ahfa74@yahoo.com, eng_mah75@yahoo.com

ABSTRACT
Three-dimensional CFD simulations are carried out to investigate heat transfer and fluid flow characteristics of a two-row plain fin-and-tube heat exchanger using Open FOAM, an open-source CFD code. Heat transfer and pressure drop characteristics of the heat exchanger are investigated for Reynolds numbers ranging from 330 to 7000. Model geometry is created, meshed, calculated, and post-processed using open source software. Fluid flow and heat transfer are simulated and results compared using both laminar and turbulent flow models (k-epsilon, and Menter SST k-omega), with steady-state solvers to calculate pressure drop, flow, and temperature fields. Model validation is carried out by comparing the simulated case friction factor f and Colburn factor j to experimental results from the literature. For friction factor determination, little difference is found between the flow models simulating laminar flow, while in transitional flow, the laminar flow model produced the most accurate results and the k-omega SST turbulence model was more accurate in turbulent flow regimes. The most accurate simulations for heat transfer in laminar flow are found using the laminar flow model, while heat transfer in transitional flow is best represented with the SST k-omega turbulence model, and heat transfer in turbulent flow is more accurately simulated with the k-epsilon turbulence model. Reasonable agreement is found between the simulations and experimental data, and the open-source software has been sufficient for simulating the flow fields in tube-fin heat exchangers.

Keyword: model, tube-fin heat exchanger, CFD simulation, heat transfer, fluid flow characteristics.

INTRODUCTION
Vestas Aircoil A/S produces compact tube-and-fin heat exchangers for ship motors, as well as other types of heat exchangers and cooling towers (Figure-1). The heat exchanger cools heated, compressed air from the motor with cooling water. Fins are used to increase heat transfer area on the air side, since the air has the largest influence on the overall heat transfer resistance.

Figure-1. Vestas air coil A/S heat exchanger and close-up of fin-and-tube arrangement.

Open-source CFD code Open FOAM is used for this study, since other commercial codes such as Fluent and Ansys CFX require expensive license fees which are so high as to be prohibitive for most small- and medium-sized companies to justify the cost. With open-source code, the only costs are the computer hardware and the engineer’s time used for setting up the case.

This study involves building a model of a fin-and-tube heat exchanger geometry using open-source software, creating a suitable mesh, setting up the cases (choosing solvers, numerical solution methods, etc.), making the CFD calculations with Open FOAM, and comparing results to known experimental data. Since the data available from previous Vestas Air coil A/S testing is confidential and not necessarily comprehensive enough for CFD validation, experiments done on fin-and-tube heat exchangers and reported in the literature are used for validation.

The following subsections describe this study in more details. First, a summary of other research in the heat-transfer field related to tube-and-fin heat exchangers is presented to put this study into perspective with the other work available in the open literature.

Previous research and experiments
This study is a CFD simulation of the heat transfer and fluid flow of a two-row heat exchanger previously tested experimentally and reported in the literature. Three studies were found in the literature search which used CFD to simulate flow and heat transfer in tube-and-fin heat exchangers. All of them used the Fluent CFD program and were directed at comparing the heat transfer and pressure drop of heat exchangers with

different geometrical characteristics [Erek *et al*., 2005], [Sahin *et al*., 2007], [Tutar and Akkoca, 2002], [Wang *et al*., 2006] describes experimental results from 15 heat exchangers of different geometrical parameters such as number of tube rows, fin spacing and fin thickness. In the experiments, heat exchangers were tested with an induced flow open wind tunnel, and results presented in graphs of friction factor and Colburn j-factor against Reynolds numbers.

This is the study used for validation (with experimental details described later in this section). [Kayansayan 1994] characterized heat-transfer in tube-and-fin heat exchangers for 10 configurations for Reynolds numbers ranging from 100 to 30,000, with the Reynolds number characteristic dimension being the tube collar thickness, and studied in particular the effect of fins on heat transfer. [Yan and Sheen 1999] made a study to compare plate, wavy, and louvered fin-and-tube heat transfer and pressure drop characteristics using different evaluation methods for the air side performance. [Ay *et al*, 2002] had deled with Infrared thermo graphic experiments to characterize the temperature distribution on the fins and calculate fin local convective heat transfer coefficients of staggered and in-line tube-and-fin heat exchanger arrangements. [Rocha *et al*., ….] A 2D second-order finite differencing analysis on one-and two-row tube-and-fin heat exchangers has been carried out to compare heat transfer and pressure drop between exchangers containing circular and elliptical tubes. Analytical methods for determining fin efficiency have been compared using 2D SimTherm® software for numerically solving the heat conduction equation. [Chen *et al*., 2006] he had used finite differencing for estimating the heat transfer coefficient on the fins. [Tao *et al*., 2007] developed a 3-D code to study fin-and-tube heat exchangers, using a body-fitted coordinate system based on the Poisson equation.

There were no articles in the literature found regarding the use of open-source CFD software Open FOAM to simulate tube-and-fin heat exchangers. However, there has been work done by [Mangani *et al*., 2007] to study the development and validation of the CFD computational code used in the Open FOAM software. It was determined in this study that the Open FOAM libraries accurately reproduced flow conditions, a conclusion which was verified with both experimental data and commonly used commercial software. The literature review has shown that virtually no CFD simulations on tube-and-fin heat exchangers using Open FOAM have been published in the open literature. Furthermore, the CFD studies found all dealt with the effect of geometrical parameters on the heat transfer and pressure drop characteristics. In this study of tube-and-fin heat exchangers, the simulation results from just one heat exchanger geometrical configuration: a two-row, staggered tube-and-fin arrangement, simulating pressure drop and heat flow for a range of Reynolds numbers from approximately 330 to 7000. However, for this study, the CFD simulations are carried out using the open-source CFD software Open FOAM, and different flow models are used for simulations: a laminar flow model and turbulence models *k-epsilon* and SST *k-omega*.

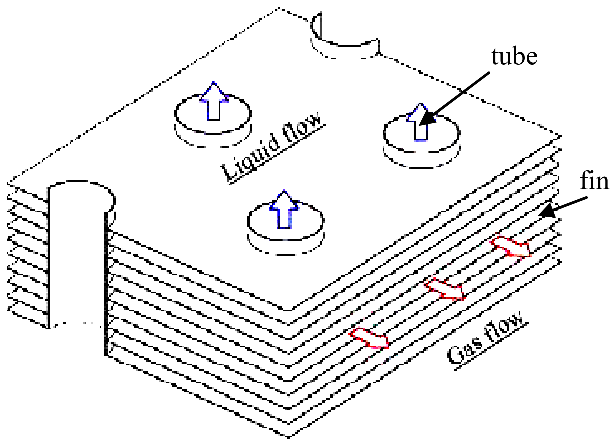

Figure-2. Typical fin-and-tube heat exchanger section with staggered tube arrangement. [Song and Nishino, 2008].

Experimental work

The experiments carried out by *Wang et al., (1996)* were conducted using a forced draft wind tunnel (Figure-3). An air straightener was used to keep flow moving in the *x*-direction, an 8-thermocouple mesh was placed in the inlet and a16-thermocouple mesh in the outlet (locations of which determined by ASHRAE recommendations [ASHRAE, 2009]. All equipment for data acquisition (thermocouples, pressure transducer, airflow measurement station, and flow meter were checked for accuracy prior to running the experiments.

Water at the inlet was held at 60ºC, air flow velocities were tested in the range from 0.3 m/s to 6.2 m/s. Energy balances were monitored during the experiment for both the hot- and cold-side and reported to be within 2.

The uncertainties for the primary measurements (mass flow rate for air and water, pressure drop, and temperature of the water and air) were very small and therefore these measurements can be assumed to be accurate.

For this experimental study, the geometrical parameters for a two-row heat exchanger based on experimental research [Wang *et al*., 1996] are used to build a CFD model, and results read from the graphs (friction factor and Colburn *j*-factor against Reynolds number) in the article are used to validate the results of the CFD simulations. The parameters of interest: friction factor *f* and Colburn *j*-factor are widely used in industry to characterize pressure drop and heat transfer, respectively, and thereby determine heat exchanger performance and suitability for specific duties. Determining and using these parameters for performance prediction is part of the heat exchanger design process.

VOL. 6, NO. 7, JULY 2011 ISSN 1819-6608
ARPN Journal of Engineering and Applied Sciences

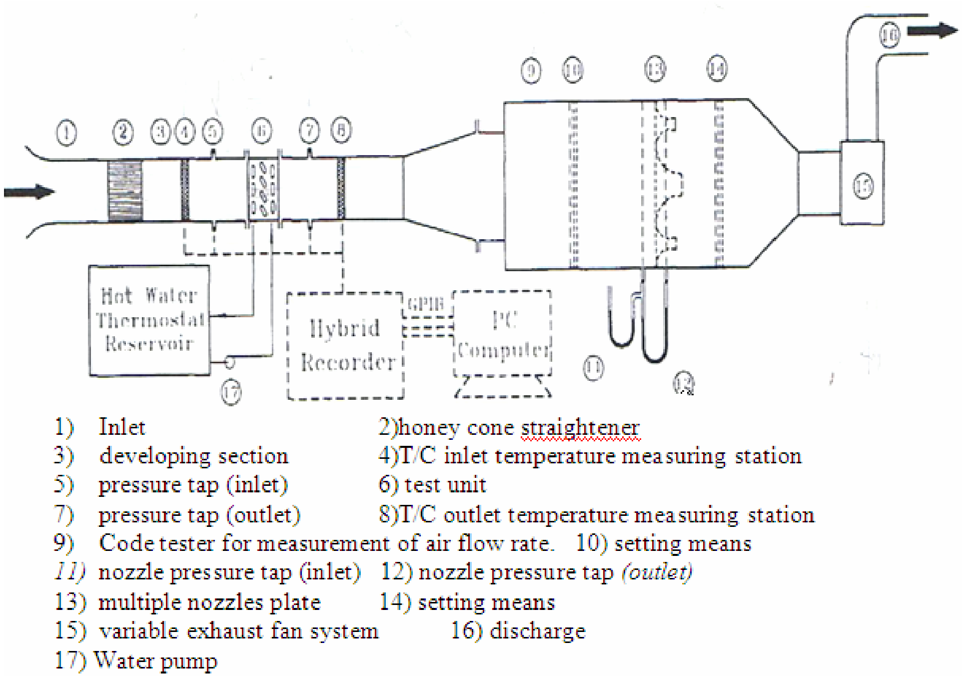

Figure-3. Illustration of experimental set-up for heat exchanger testing [Wang *et al*., 1996].

The two-row fin-and-tube heat exchanger studied has a staggered tube arrangement, as illustrated in Figure-3. Analyzing flow and heat transfer using CFD can make calculations to predict heat-exchanger performance. However, it is not possible to perform CFD simulation on the entire heat exchanger, due to the large number of volumes and calculations required. Therefore, a small section of a heat exchanger consisting of one channel of air between two fins, with the air flowing by two tubes is modelled for this project. Simulations of the air flow through this passage are carried out, while relevant characteristics of the air flow are sampled and averaged at the inflow, minimum free-flow area (s), and outflow. The characteristics sampled are: flow velocity (in all three directions: x, y, and z), temperature, pressure, and turbulence model parameters *k*, *epsilon*, and *omega*. These measurements are then used for calculating relevant performance parameters such as pressure drop, friction and Colburn factors, heat transfer rate, Reynold's number, etc.

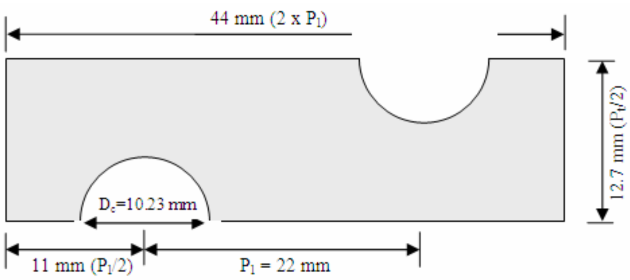

Figure-4. Illustration of the main computational domain and geometric parameters of the heat exchanger model studied (z-direction not shown).

Computational domain and boundary conditions

The pre-processing open-source software Salomé is used to create and mesh the computational model. A diagram of the studied model is shown in Figure-4, and consists of the air flow area between two fins of plain fin geometry and around the surfaces of two rows of tubes, and a schematic of the model with dimensions is shown in Figure-5, with the geometrical values listed in Table-1.

Table-1. Geometric dimensions of heat exchanger model.

Geometric parameter	
Fin thickness t	*0.130 mm*
Fin pitch F_p	*2.240 mm*
Fin collar outside diameter D_c	*10.23 mm*
Transverse pitch P_t	*25.40 mm*
Longitudinal Pitch P_l	*22.00 mm*
Tube wall thickness δ	*0.336 mm*
Number of tube rows	*2*

The computational domain is actually 8 times the original heat transfer area (as illustrated in Figure-5), and is defined by $0 < x < 8P_l$, $0 < y < P_t/2$, and $0 < z < F_p$., while the actual modelled heat exchanger length is equal to twice the longitudinal pitch P_l. The volume representing the air which passes through the gap between the two fins is extended upstream from the inlet and downstream from the outlet in order to reduce oscillations and ensure a representative flow in the computational domain of the actual heat exchanger. The heat exchanger model with its extended volume is illustrated in Figure-5, while the actual

ARPN Journal of Engineering and Applied Sciences

www.arpnjournals.com

area of interest for the heat exchanger simulation is shown later in Figure-9 (and the middle section of Figure-5).

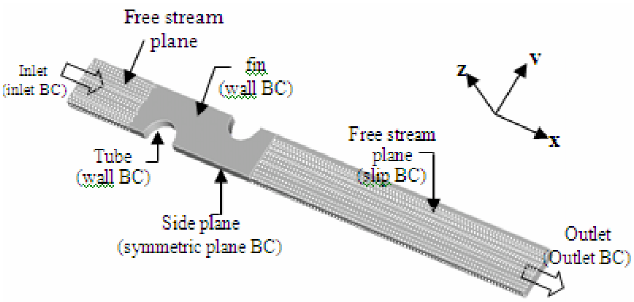

Figure-5. Computational domain, including boundary conditions (BC) and extended flow volumes.

The computational domain has contains boundary conditions as shown in Figure-5 with the following conditions:

Tube surfaces, Dirichlet BC:

$T = T_w$,

Air velocity: $u = v = w = 0.$

Fins, Dirichlet BC:

$T = T_{fw}$

Air velocity: $u = v = w = 0$

Inlet, Dirichlet BC:

Uniform velocity $u = u_{in}$,

$v = w = 0$

$T = 5$ ºC.

Outlet, Neuman BC:

Zero gradients, u, v, w, pressure, and temperature. (One-way),

Free stream planes: (top and bottom planes of the extended surface areas):
'slip' conditions?: $(\partial u/\partial z)=0$, $(\partial v/\partial z)= 0$, $w= 0$,$(\partial T/\partial z)= 0.$

Side planes: symmetry planes

$(\partial u/\partial y)=0$, $v = 0$, $(\partial w/\partial y) = 0$, $(\partial T/\partial y) = 0$

The entire computational domain was made up of 50,375 finite volumes, with a structured grid throughout most of the domain, while the areas around the tubes are more unstructured.

CFD governing equations

The element has dimensions δx, δy, *and* δz, with the center point at (x, y, z) and six faces N, S, E, W, T and B (North, South, East, West, Top, Bottom). Each fluid property (velocity, pressure, density, viscosity, thermal conductivity, and temperature) therefore can be represented as a function of space and time with:

$\bar{u}(x, y, z, t)$, $p(x, y, z, t)$, $\rho(x, y, z, t)$, $\mu(x, y, z, t)$, $k(x, y, z, t)$, and $T(x, y, z, t)$.

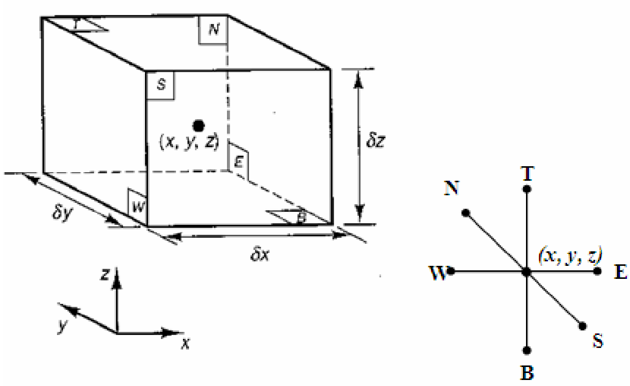

Figure-6. CFD Fluid element for calculating changes in fluid property, coordinate systems in three dimensions x, y, z, and according to faces N, S, E, W, T and B. [Hjertager, 2007], [Versteeg and Malalasekera, 2007].

Mass balance (Continuity equation): *"Fluid mass is conserved."*

Equation 1

$$\frac{\partial \rho}{\partial t}+\frac{\partial(\rho u)}{\partial x}+\frac{\partial(\rho v)}{\partial y}+\frac{\partial(\rho w)}{\partial z}=0$$

also written as $$\frac{\partial \rho}{\partial t}+div(\rho\vec{u})=0$$

or $d\dot{m}=\sum\delta\dot{m}_{in}-\sum\delta\dot{m}_{out}$ which can be summarised as:

[mass accumulation over time] = [sum of all inflows] - [sum of all outflows]
Where δ represents area, and can be illustrated in the following diagram.

Before presenting the remaining 7 equations, a brief illustration of how Equation 1 was derived is given here. The momentum and energy balances are derived similarly for a fluid element. Therefore instead of writing them out in detail, only the summary of equations expressions will be given, and for details of the derivation, similarities can be assumed with the following mass balance illustration shown here.

Consider an element similar to that shown in Figure-7. The fluid element's rate of mass increase is:

Equation 2 $$\frac{\partial}{\partial t}(\rho\delta x\delta y\delta z)=\frac{\partial \rho}{\partial t}(\delta x\delta y\delta z)$$

The net rate of flow is the sum of mass inflow subtracted by the sum of mass outflow. The first two terms of a Taylor series expansion can accurately express fluid properties at the faces. Therefore, the mass flow in the x-direction through the W and E faces (at a distance of $(1/2)*(\delta x)$ from the center of the element) is expressed as:

ISSN 1819-6608
ARPN Journal of Engineering and Applied Sciences

www.arpnjournals.com

$\rho u - \frac{\partial(\rho u)}{\partial x} \cdot \frac{1}{2} \delta x$ for the west face W, and $\rho u + \frac{\partial(\rho u)}{\partial x} \cdot \frac{1}{2} \delta x$ for the east face E.

The mass flow in the y-direction through the S and N faces and in the z-direction through the B and T faces can be similarly expressed. All of these are illustrated in Figure-7 and summarized after the illustration using Equation 3.

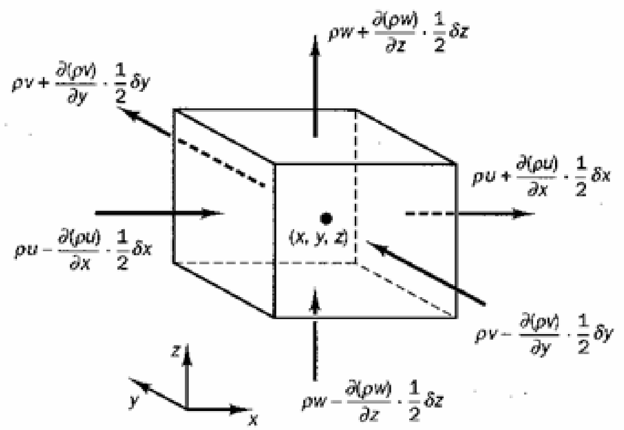

Figure-7. Fluid element illustrating flows of inflows and outflows of mass on all six faces. [Versteeg and Malalasekera, 2007].

As can be seen in Figure-7, the overall mass flow rate across the element's faces is represented by the following expression, in which the entire control volume is taken into account by multiplying the mass rate in a particular direction by the two remaining dimensions:

Equation 3 Net mass flow =

$$\left(\rho u - \frac{\partial(\rho u)}{\partial x} \cdot \frac{1}{2} \delta x\right) \delta y \delta z - \left(\rho u + \frac{\partial(\rho u)}{\partial x} \cdot \frac{1}{2} \delta x\right) \delta y \delta z$$
$$+ \left(\rho v - \frac{\partial(\rho v)}{\partial y} \cdot \frac{1}{2} \delta x\right) \delta x \delta z - \left(\rho v - \frac{\partial(\rho v)}{\partial y} \cdot \frac{1}{2} \delta x\right) \delta x \delta z$$
$$+ \left(\rho w - \frac{\partial(\rho u)}{\partial z} \cdot \frac{1}{2} \delta x\right) \delta x \delta y - \left(\rho w - \frac{\partial(\rho u)}{\partial z} \cdot \frac{1}{2} \delta x\right) \delta x \delta y$$

Equation 2 (rate of increase of mass inside the element) is equated to Equation 3 (net mass flow rate into the control volume across its faces). The terms are arranged on the left side of the equation, and divided by the control volume $\left(\delta x \delta y \delta z\right)$ to get the continuity equation for compressible fluids:

$$\frac{\partial \rho}{\partial t} + \frac{\partial(\rho u)}{\partial x} + \frac{\partial(\rho v)}{\partial y} + \frac{\partial(\rho w)}{\partial z} = 0$$

If the fluid is incompressible, the density is constant and equation becomes div $\vec{u}$ = 0.

Equation integration and discretisation

A steady-state one-dimensional heat transfer through diffusion is governed by the general transport equation (Equation 4). When the transient and convective terms are deleted, the equation becomes:

Equation 4

$$\frac{\partial}{\partial x_i}\left[\Gamma_\varphi \frac{\partial \varphi}{\partial x_i}\right] + S_\varphi = 0 \quad \text{or} \quad div(\Gamma_\varphi grad \varphi) + S_\varphi = 0$$

Integration of Equation 4 yields:

Equation 5

$$\int_{CV} div(\Gamma_\varphi grad \varphi) dV + \int_{CV} S_\varphi dV$$
$$= \int_A \vec{n} \;.\; (\Gamma_\varphi grad \varphi) dA + \int_{CV} S_\varphi dV = 0$$

In the one-dimensional steady-state heat transfer diffusion problem, the equation becomes:

Equation 6 $$\frac{d}{dx}\left[\Gamma \frac{d\varphi}{dx}\right] + S = 0$$

Where enthalpy $h = \varphi$

$$= \int_{T_{ref}}^{T} C_p dT = C_{pm}\left(T - T_{ref}\right), \quad C_{pm} = \frac{\int_{T_{ref}}^{T} C_p dT}{(T - T_{ref})}$$ and

$\Gamma_h = k / C_{pm}$

It can be seen from the expressions above, that the enthalpy is the scalar property to be transported. The transport coefficient for Γ enthalpy is the thermal conductivity k divided by the specific heat capacity C_{pm} at the average temperature of the cell. The rate of heat transfer by diffusion (term (III) in the transport equation), is then:

$\frac{\partial}{\partial x}\left[\frac{k}{C_{pm}} \frac{\partial}{\partial x}(C_{pm}(T - T_{ref}))\right]$, and the transport equation to use is

Equation 7

$$\frac{\partial}{\partial x}\left[\frac{k}{C_{pm}} \frac{\partial}{\partial x}(C_{pm}(T - T_{ref}))\right] + S_\varphi = \frac{\partial}{\partial x}\left[k \frac{\partial T}{\partial x}\right] + S_\varphi = 0$$

Equation 7 is the one-dimensional energy equation, to be discretised and solved for diffusion.

Grid Generation

To discretise the energy equation over the fluid elements in a computational domain, the following single fluid element is illustrated:

ARPN Journal of Engineering and Applied Sciences

www.arpnjournals.com

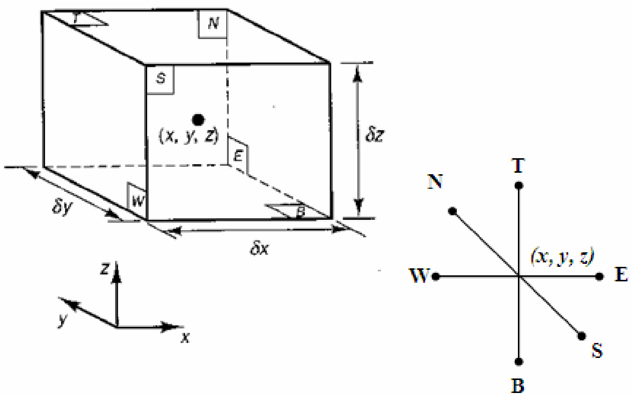

Figure-8. CFD Fluid element for calculating changes in fluid property, with two coordinate systems in three dimensions x, y, z, and according to faces N, S, E, W, T and B. [Hj ertager, 2007] [Versteeg and Malalasekera, 2007]

In the heat diffusion problem, heat flow in three dimensions (N-S, W-E, T-B) is explained. Therefore, one row of fluid elements, each with a central node like the one above, is illustrated.

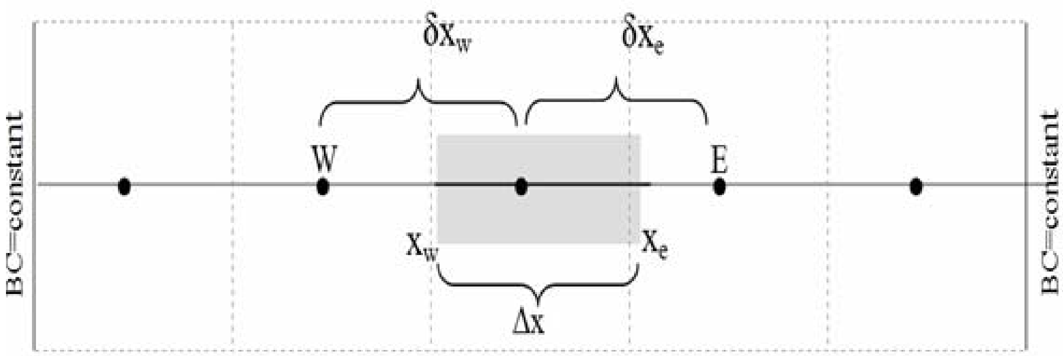

Figure-9. One-dimensional grid with nodal points.

Discretisation

In three-dimensional calculations, a similar set-up is made for the N, S, T, and B faces and corresponding central nodes. For a one-dimensional calculation, the integration from the west and east faces on either side of node P is carried out according to equation 5, resulting in Equation 8:

Equation 8

$$\int_A \vec{n} \,.\, (\Gamma_\varphi grad\varphi) dA + \int_{CV} S_\varphi dV =$$

$$\int_{x_w}^{x_e} \frac{d}{dx}\left[kA\frac{dT}{dx}\right]dx + \int_{x_w}^{x_e} S_\varphi dV = \left[kA\frac{dT}{dx}\right]_{x_e} - \left[kA\frac{dT}{dx}\right]_{x_w} + \bar{S}\Delta V = 0$$

Where A is the cross-sectional area of the fluid element, ΔV is the volume and $\bar{S}$ the average source in the fluid element.

As seen in Equation 8, the governing equation is integrated across the fluid element, with node P described with a discretised equation.

Temperature gradients at x_e and x_w must be known for Equation 9 to be useful. The temperature T (or other scalar property φ) and thermal conductivity k (or diffusion coefficient Γ) are determined for the nodes, and therefore the property value gradients at the faces x_e (halfway between nodes P and E) and x_w (between nodes W and P) between must be approximated. There are different types of differencing schemes for this purpose.

Central differencing scheme

Direct linear averaging (assuming uniform grid) of the values can be used, which is termed the central differencing method. The other differencing methods are compared in the next section (upwind differencing, hybrid, or power-law, and other higher-order differencing schemes), and the choice made for this project given. When the differencing method is chosen (in this case central differencing), the equation takes the form:

Equation 9

$$\left[k_e \frac{T_E - T_P}{\delta x_e}\right] - \left[k_w \frac{T_P - T_W}{\delta x_w}\right] + \bar{S}\Delta V = 0$$

The equation is then rearranged with all P scalar variables on the left side, and W and E variables on the other, with specific terms given the names a_P, a_W, a_E, and b, as shown in the following equation:

Equation 10

$$\left[\frac{k_e}{\delta x_e}A_e+\frac{k_w}{\delta x_w}A_w\right]T_P=\left[\frac{k_w}{\delta x_w}A_w\right]T_W+\left[\frac{k_e}{\delta x_e}A_e\right]T_E+\bar{S}\Delta V=0$$

(a_P) (a_W) (a_E) (b)

The discretized equation with the representative terms a_P, a_W, a_E and b is then:

Equation 11

$$a_PT_P=a_WT_W+a_ET_E+b$$

for a three-dimensional problem, a similar expression is found for the N, S, T, and B faces:

$$a_PT_P=a_WT_W+a_ET_E++a_ST_S+a_NT_N+a_TT_T+a_BT_B+b$$

If the problem includes convection in addition to diffusion, the coefficients for *a* will include an additional term to account for the convection. For example, *F* could represent convective mass flux (*ρu)*, while D represents the diffusion conductance (*k/δx*) resulting in a_W now being equated to $[D_w+(F_w/2)]$.

The central differencing scheme does not always reach correct solutions when both convection and diffusion forces are involved.

The simple algorithm

The SIMPLE algorithm is a guess-and-correct technique to determine the values for pressure on a staggered grid. It is iterative and must be done in the specific order when other scalars are also calculated. The general procedure for the technique is shown in Figure-10.

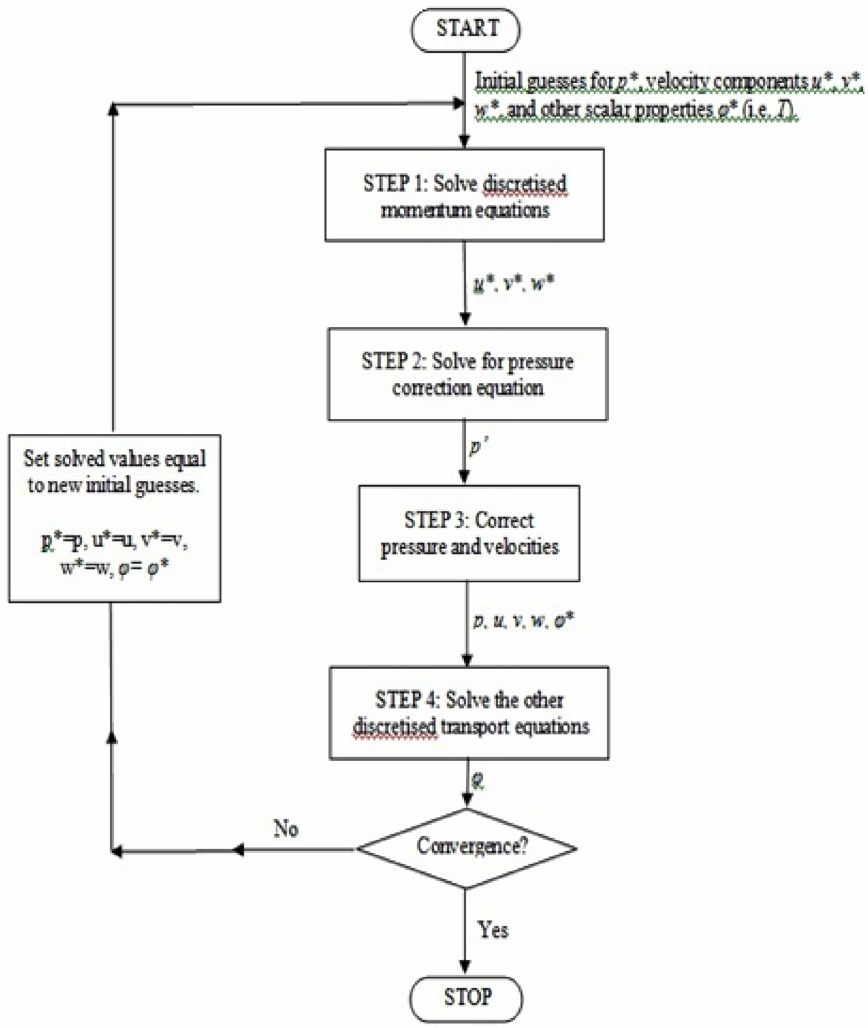

Figure-10. The simple algorithm [Hjertager, 2007], [Versteeg and Malalasekera, 2007].

RESULTS

This section describes the initial observations found using para-View after running the CFD simulations in Open FOAM. The characteristics of low-Reynolds flow and high-Reynolds flow are compared with contour plots of velocity with vectors (Figures 11 and 12), and contour plot of turbulent kinetic energy *k* (Figures 13 and 14).

The highest velocity areas are just off the streamlines flowing directly around the tubes, and located at the area of minimum free-flow. In the case of the case

VOL. 6, NO. 7, JULY 2011 ISSN 1819-6608
ARPN Journal of Engineering and Applied Sciences

with inlet velocity of 0.3 m/s, the top velocity at the second tube is 0.88 m/s, nearly 3 times the inlet velocity. For the 6.2 m/s inlet flow case, the top velocity reaches 15 m/s, more than twice the inlet velocity.

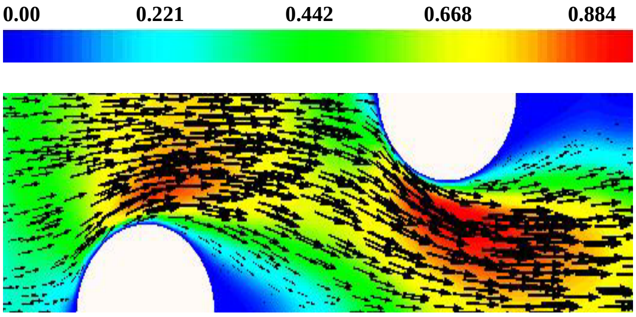

Figure-11. Contours and vector plot for U velocity field, SST k-omega flow model, inlet air flow 0.3 m/s.

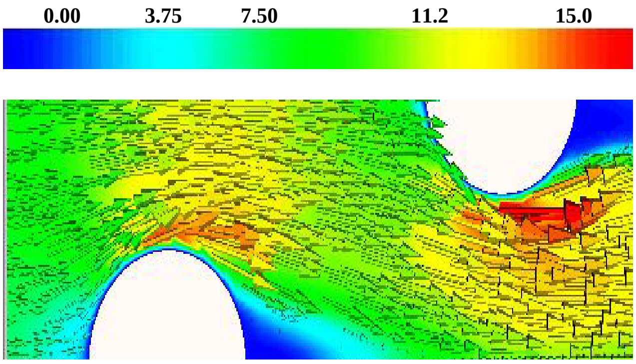

Figure-12. Contours and vector plot for U velocity field, SST k-omega flow model, inlet air flow 6.2 m/s.

The kinetic energy contour plots can be seen to verify previous observations made regarding flow. It is seen in Figure-13, which illustrates the kinetic energy k distribution for the low Reynolds number case. There is no kinetic energy increase in the areas behind the tubes for this case. The kinetic energy increases (slightly) in a different area corresponding to the increase in velocity as the air flows around the second tube.

The other area of Figure-13, the plot of lower Reynolds number, which is exhibiting higher kinetic energy, is in the area of higher temperatures, which can be seen from the graph in Figure-10. However, this illustrates that even at very low flow rates; some turbulent kinetic energy could still be present.

For kinetic energy in the higher-Reynolds number case, an increase in kinetic energy is found clearly after the first tube, in the same area as the recirculation zones observed in the higher Reynolds values. According to this plot, then, the second recirculation zone is not as turbulent as the first recirculation zone. This makes sense because the direction of flow has changed as the air moves between the two tubes, and is directed more 'downward' at an angle (as shown by the vectors in Figure-13. The flow rounds the tube at an angle making less of an impact with the tube and 'missing' the recirculation zone.

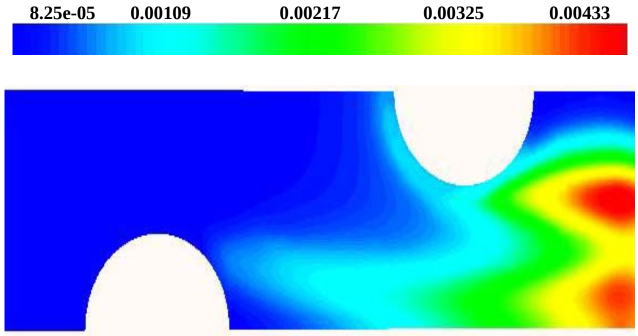

Figure-13. Contours of turbulent kinetic energy k distribution, SST k-omega model, inlet air velocity 0.3 m/s.

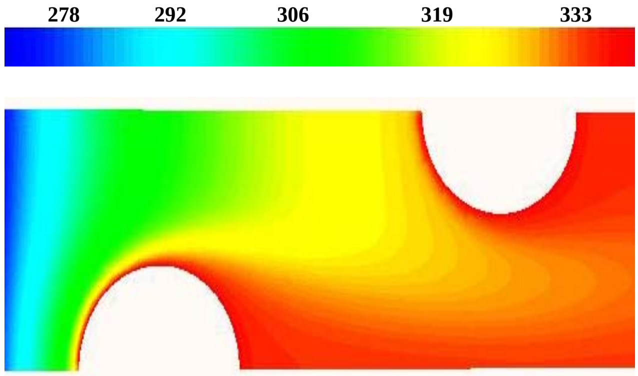

Figure-14. Contours of temperature field, SST k-omega flow model, 0.3 m/s inlet air velocity.

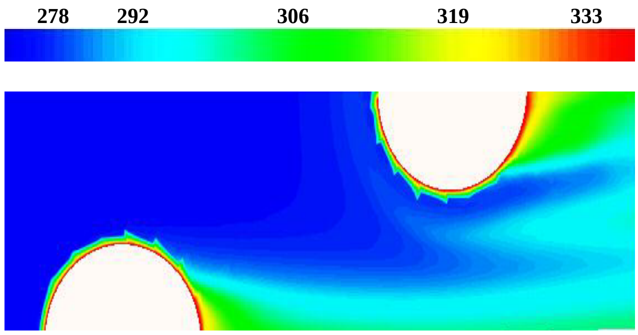

Figure-15. Contours of temperature field, SST k-omega flow model, 6.2 m/s inlet air velocity.

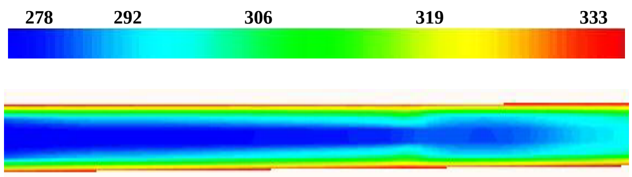

Figure-16. Contours of temperature Field SST k-omega flow model, z-direction, 6.2 m/s inlet air velocity.

The first most noticeable difference between the two Reynolds number heat transfer characteristics is that once steady-state is reached, the slower-moving air (0.3 m/s) is heated up much more in the first two rows than in the case of higher Reynolds number flows. This must be due to the fact that the air flows so slowly, that there is much more time to absorb the heat (longer 'residence time'). Had the initial inlet conditions been made cyclical, then comparisons could be made deeper into the heat exchanger (for example after 10 or 12 rows) and see how the heat transfer compares.

Although streamlines are not physically drawn onto Figures 15 and 16, they can be seen fairly clearly with the colour contrast lines. It is seen that the temperature streamlines run practically perpendicular to the velocity streamlines in the beginning of the airflow channel, with the isothermal streamlines running vertical and the velocity of the flow horizontal.

It can be seen in Figure-16 that the higher Reynolds number flow has not only a lower temperature change than the previous example, but also a different pattern (different kinds of isothermal streamlines). The largest temperature changes for this case are occurring in the recirculation and 'slow velocity' zones (shown previously in the vector and velocity contour plot) just after each of the tubes. As in the slow-moving flow in the case with 0.3 m/s velocity, the slow-moving areas of the heat exchanger are also better able to absorb heat. The staggered tube arrangement is designed to have these slower-moving and recirculation areas to keep the heat flowing to the air, but at the same time, not allowing recirculation zones to 'stagnate' as can occur in inline arrangements where these zones do not keep flowing [Jang *et al*., 1995].

Figure-16 shows the contours across the z-direction in the middle of the airflow channel (which flows directly between the two tubes). It can be seen that the fins on the top and bottom are heated, and only a very thin 'boundary' layer of air has time to be heated after first entering the channel. It can be seen where the flow with heat from the first tube warms up the air, but then flows away again as all the air flow has to go around the second tube.

DISCUSSIONS

Simulations for this project were carried out following as closely as possible the same operating conditions and geometrical configurations of the two-row tube-fin heat exchanger, with tube collar diameter of 10.23 mm and fin pitch 2.23 mm, as presented in the paper by [Wang *et al*., 1996]. The Reynolds number ranges from 330 to 7000, which correspond to the frontal air velocity at the inlet ranging from 0.3 to 6.2 m/s.

The work done for this study has shown that it is possible to make practical simulations of heat flow and pressure drop for a tube-and-fin heat exchanger using open source CFD software, and validate the results against experimental data. Data resulting from the simulations should be as accurate as possible, and therefore some considerations can be taken in future work to attempt to further improve the simulation conditions/calculations and the accuracy of the results. These improvements could include changes to the following areas of CFD simulation: A more comprehensive grid independence test.

Changes to the fin temperature based on fin effectiveness calculations. The efficiency equation given in [Baggio and Fornasieri; 1994] assumes a uniform air and fin temperature, which is not the case in this project. As shown by [Ay *et al*., 2001] and results from infrared thermography measurements, the local convective heat transfer coefficient changes across the fin according to various parameters. It was shown that there is a lower temperature at the leading edge of the plate-fin, and a sharper temperature gradient on the fin surface where the boundary layer increases and destroyed as the fluid flows around the tubes (for the first two rows of tubes).

Once the flow has gone around the tubes, the temperature gradient decreases from airflow being swept into the wake. However, by the third row of tubes, the wake pattern changes again, and further variations of the heat transfer coefficient can be seen throughout the heat exchanger, with specific patterns depending on the Reynolds number (among other parameters). The article included studies of staggered and in-line fin-and-tube heat exchangers. The temperature gradients can also be studied in relation to the synergy principle presented by [Tao *et al*., 2007], where the heat transfer coefficient is shown (qualitatively) to change according to the angle of local isothermal streamlines to the temperature field. The general pattern of heat transfer coefficient in this study is similar to that described by the Baggio and Fornasieri; 1994.

Clarification of the air temperature at inlet and the hot water flow rate through the tubes, as this information was not provided in the [Wang *et al*., 1996] article.

Improve the final mesh to be used (structured vs. unstructured or hybrid, determine areas of geometry requiring finer mesh, etc.). [Versteeg and Malalasekera; 2007] suggest that non-structured grids can be more accurate and efficient than structured grids.

Use a solver for conjugated heat transfer analysis to include the interactions between the air, tube wall, and water, which have recently become available in the Open FOAM version 1.5.1.

Use cyclic boundary conditions for inlet flow to investigate pressure drop and heat flow characteristics deeper into the heat exchanger.

Use the new geometry and mesh creation program snappy Hex Mesh available now in Open FOAM (instead of Salomé, which proved difficult to use at times, and no technical support was available).

Use a low Reynolds number turbulence model to better simulate the turbulence at the lower Reynolds numbers not accurately modelled by any of the flow models.

Make more use of the open FOAM discussion boards and online information, since no technical support is available (Learn the Open FOAM more thoroughly).

VOL. 6, NO. 7, JULY 2011 ISSN 1819-6608
ARPN Journal of Engineering and Applied Sciences

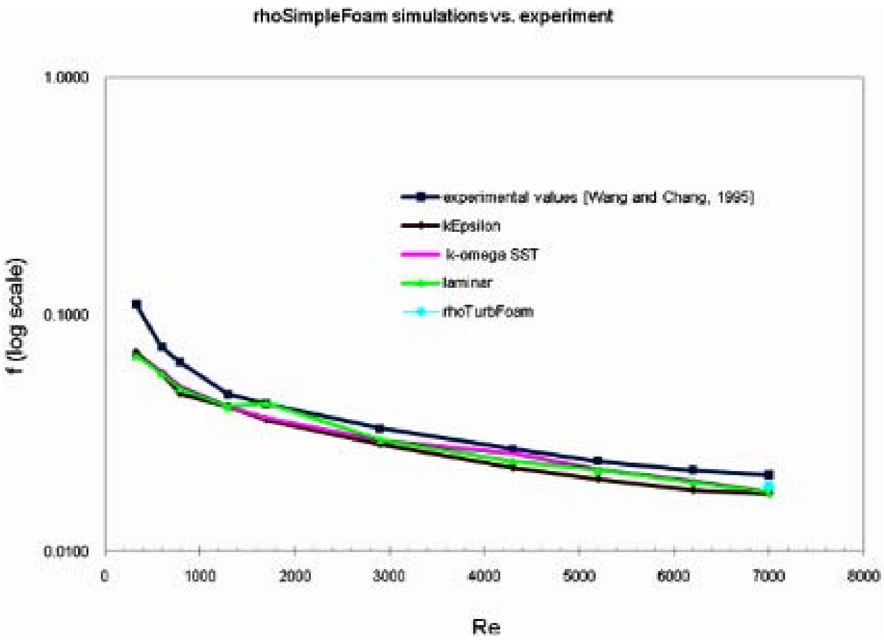

Figure-17. Fanning friction factor f against Reynolds number Re for different inlet airflow velocities and flow models (laminar, and turbulence models k-epsilon and k-omega) with the same geometrical parameters.

Possible changes to the turbulence model in Open FOAM, or solving procedures - which is possible since it is open source C++, and changes only require basic programming skills in object-oriented programming, making it relatively simple to implement new turbulence models, solver algorithms, boundary condition types, and physical models. This is an advantage over commercial software, where access to the code is unavailable.

Finally, as discussed in the book by [Kays and London; 1998], the properties of air are highly temperature-dependent, and many of the calculations do not account for these changes, but instead use an average value, which can substantially affect the flow at a particular cross section according to the temperature profile (for example in this case, flow characteristics were determined using average temperatures taken at the inlet and outlet).

Run the steady-state versions of *k-omega* turbulence models further to see if they can converge better, since the curve of Colburn j-factor vs. Reynolds number seems to be unstable with a noticeable fluctuation at the inlet flow velocity of 3.7 m/s (corresponding to Reynolds number 4300).

Implementation of anisotropic turbulence models to correct for the differences in flow according to the direction, i.e., use the realizable *k-epsilon* turbulence model or use of the RSM (Reynolds stress equation model) turbulence models.

As can be seen from the preceding list, which does not consider all the possible aspects, there is much to be considered for ensuring accurate simulations of the fin-and-tube heat exchangers. To summarize, considerations should be taken for: heat exchanger geometry and mesh, fin temperature, boundary conditions (air and water temperatures, and cyclic inlet), turbulence model variations, Open FOAM use and programming, convergence, and temperature-dependent properties of air. All of these considerations are subjects of interest which can be studied in the open literature as described in this paper and listed in the references.

CONCLUSIONS

The objective of this study was to make CFD simulations using open source software, and validate the results against experimental data. The system to study was a fin-and-tube heat exchanger. The purpose of the work was to investigate the possibilities of eventually using CFD calculations for design of heat exchangers instead of expensive experimental testing and prototype production. To analyse the flow and heat transfer characteristics of the heat exchanger, a model of a two-row fin-and-tube heat exchanger was created using open source Salomé software to create the geometry and mesh. The resulting mesh (after a grid independence test was carried out) was used for running a variety of simulations using a laminar flow model and two turbulence models for comparison of results. Ten different inlet flow velocities ranging from 0.3 m/s to 6.2 m/s and corresponding to Reynolds numbers ranging from 330 to 7000 were simulated in the three different flow models (laminar, *k-epsilon* turbulence model, and SST *k-omega* turbulence model). A sampling dictionary was written into the CFD model to record pressure and temperature measurements at the inlet and outlet of the heat exchanger model. Using the simulation results and some specific non-dimensional numbers, calculations related to heat flow and pressure loss can be carried out to determine the Fanning friction factor and

VOL. 6, NO. 7, JULY 2011 ISSN 1819-6608
ARPN Journal of Engineering and Applied Sciences

www.arpnjournals.com

Colburn *j*-factor for comparison with the literature values used for the validation.

It was found that the flow model accuracy depended on the flow regime and whether the friction factor *f* or *j*-factor was being determined. From the experimental values given in the literature, the laminar flow region for this particular geometry of heat exchanger switched to transitional at around Reynolds number 1300, and moving to transitional around Reynolds number 2900. The Reynolds number has a characteristic dimension of the tube collar outside diameter.

For friction factor determination, little difference is found between the flow models simulating laminar flow, while in transitional flow, the laminar flow model produced the most accurate results (for friction factor) and the SST k-omega turbulence model was more accurate in turbulent flow regimes. For heat transfer, the laminar flow model calculated the most accurate *j*-factor, while for transitional flow the SST *k-omega* turbulence model was more accurate and the *k-epsilon* turbulence model was best for heat transfer simulations of turbulent flow.

The flow model can be chosen based on what is being studied (heat flow or pressure drop) and the flow regime. In conclusion, it is found that the pressure drop and heat transfer characteristics of a fin-and-tube heat exchanger can be determined to within a reasonable accuracy with CFD computations carried out in open source software, and that Open FOAM can be used to carry out practical work in the design process of heat exchangers.

Nomenclature

A	Area	[m^2]	N	Number of tube row	
A_o	Total surface area	[m^2]	$\dot{m}$	Mass flow rate (mass*velocity)	[kg/s]
A_{to}	External tube surface area	[m^2]	Nu	Nusselt number: $h/(k/D_h)$	
C	Heat capacity rate	[W/K]	Δp	Pressure drop	[Pa]
C_p	Specific heat	[J/kg K]	F_p	Fin pitch	[m]
D_c	Fin collar outside diameter	[m]	P_l	Longitudinal pitch	[m]
D_i	Inside tube diameter	[m]	Pr	Prandtl number: $\mu C_p/k$	
D_o	Tube outside diameter	[m]	P_t	Transverse pitch	[m]
D_h	Hydraulic diameter	[m]	$\dot{Q}$	Heat-transfer rate	[W]
f	Friction factor		r_c	Tube outside radius	[m]
G_c	Mass flux of air based on minimum flow area	[kg m^2/s]	Re	Reynolds number: $(\rho*V*D)/\mu$	
H	Fin spacing	[m]	R_{eq}	Equiv. radius for circular fin	[m]
h	Heat-transfer coefficient	[W/m^2 K]	r	Tube inside radius	[m]
j	Colburn factor: $Nu/RePr^{1/3}$		t	Fin thickness	[m]
k	Thermal conductivity	[W/m^{2}K]	T	Temperature	[°C]
K_c	Abrupt contraction pressure-loss coefficient		U	Overall heat-transfer coefficient	[W/m^2 K]
K_e	Abrupt expansion pressure-loss coefficient		X_L	$\sqrt{(P_t/2)^2 + P_t^2/2}$	[m]
L	Depth of heat exchanger in airflow direction	[m]	X_M	$P_t/2$	[m]
Subscripts			*max*	Maximum value	
1	Air side inlet		*o*	Total surface	
2	Air side outlet		*out*	Outlet	
air	Air side		*water*	Water side	
ave	Average value		*w*	Wall of tube	
b	Base surface		***Greek Letters***		
i	Tube side		δ	Tube wall thickness	[m]
in	Inlet		μ	Dynamic viscosity	[kg/ms]
f	Fin surface		ρ	Density	[kg/m^3]
m	Mean value		σ	Contraction ratio of cross-sectional area	
min	Minimum value				

REFERENCES

ASHRAE. 2009. Handbook Fundamentals. SI Edition.

Ay Herchang, Jang Jiin Yuh, Yeh Jer-Nan. 2002. Local heat transfer measurements of plate finned-tube heat exchangers by infrared thermography. International Journal of Heat and Mass Transfer. 45: 4069-4078.

Baggio P., Fornasieri E. 1994. Air-side heat transfer and flow friction: theoretical aspects. In Recent developments in finned tube heat exchangers. Energy Technology. pp. 91-159

Chen Han-Taw; Chou Juei-Che; Wang Hung-Chih. 2006. Estimation of heat transfer coefficient on the vertical plate fin of finned-tube heat exchangers for various air speeds and fin spacings. International Journal of Heat and Mass Transfer. 50: 45-57.

Erek Aytunc, Õzerdem Baris, Bilir Levent, Ilken Zafer. 2005. Effect of geometrical parameters on heat transfer and pressure drop characteristics of plate fin and tube heat exchangers. Applied Thermal Engineering. 25: 2421-2431.

Gray D. L., Webb R.L. 1986. Heat transfer and friction correlations for plate fin-and-tube heat exchangers having plain fins. Proceedings of the Ninth International Heat Transfer Conference, San Francisco.

Hjertager Bjørn H. 2007. Computational Analysis of Fluid Flow Processes. Lecture Notes, Aalborg University Esbjerg, Denmark.

Jang Jiin-Yuh, Wu Mu-Cheng, Chang Wen-jeng. 1996. Numerical and experimental studies of three-dimensional plate-fin and tube heat exchangers. International Journal of Heat and Mass Transfer. 39(14): 3057-3066.

Kayansayan N. 1994. Heat transfer characterization of plate fin-tube heat exchangers. International Journal of Refrigeration. 17(1): 49-57.

Kays W.M., London A.L. 1998. Compact Heat Exchangers. Sub-edition 3, Krieger Publishing Company, New York.

Mangani L., Bianchini C., Andreini A., Vacchini B. 2007. Development and validation of a C++ object oriented CFD code for heat transfer analysis. ASME-JSME 2007 Thermal Engineering and Summer Heat Transfer Converence, Vancouver, Canada.

McQuiston F. C. 1978. Correlation for heat, mass and momentum transport coefficients for plate-fin-tube heat transfer surfaces with staggered tube. ASHRAE Trans. 84: 294-309.

Rocha L. A. O., Saboya F. E. M., Vargas J. V. C. 1997. A comparative study of elliptical and circular sections in one- and two-row tubes and plate fin heat exchangers. International Jouernal of Heat and Fluid Flow. 18: 247-252.

Song Gil-Dal, Nishino Koichi. 2008. Numerical Investigation for Net Enhancement in Thermal-Hydraulic Performance of Compact Fin-Tube Heat Exchangers with Vortex Generators. Journal of Thermal Science and Technology. 3(2): 368-380.

Sahin Haci Mehmet, Dal Ali Riza, Baysal Esref. 2007. 3-D Numerical study on the correlation between variable inclined fin angles and thermal behaviour in plate fin-tube heat exchanger. Applied Thermal Engineering. 27: 1806-1816.

Tao Y. B., He Y. L., Huang J., Wu Z. G., Tao W. Q. 2007. Three-dimensional numerical study of wavy fin-and-tube heat exchangers and field synergy principle analysis. International Journal of Heat and Mass Transfer. 50: 1163-1175.

Tennekes H., Lumley J. L. 1972. A First Course in Turbulence. MIT Press, Cambridge, MA.

Tutar Mustafa, Akkoca Azize. 2002. A computational study of effects of different geometrical parameters on heat transfer and fluid flow in a wavy and plain fin and tube heat exchanger. Proceedings of ESDA2002: 6th Biennial Conference on Engineering Systems Design and Analysis, Instanbul, Turkey.

Versteeg H K, Malalasekera W. 2007. An Introduction to Computational Fluid Dynamics, the Finite Volume Method. Second edition, Pearson Education Limited, Essex, England.

Yan Wei-Mon, Sheen Pay-Jen. 2000. Heat transfer and friction characteristics of fin-and-tube heat exchangers. 43: 1651-1659.

Wang Chi-Chuan, Chang Yu-Juei, Hsieh Yi-Chung, Lin Yur-Tsai. 1996. Sensible heat and friction characteristics of plate fin-and-tube heat exchangers having plane fins. International Journal of Refrigeration. 19(4): 223-230.